THE JOURNAL OF PHYSICAL CHEMISTRY C

Article

pubs.acs.org/JPCC

# Single Collision Events of Conductive Nanoparticles Driven by Migration

Jun Hui Park,[⊥] Aliaksei Boika, Hyun S. Park, Heung Chan Lee, and Allen J. Bard*

Center for Electrochemistry, Department of Chemistry and Biochemistry, The University of Texas at Austin, Austin, Texas 78712, United States

Supporting Information

**ABSTRACT:** We report that conductive single nanoparticle (NP) collisions can involve a significant component of the mass transport to the electrode of the charged NPs by migration. Previously, collision events of catalytic NPs were described as purely diffusional using random walk theory. However, the charged NP can also be attracted to the electrode by the electric field in solution (i.e., migration) thereby causing an enhancement in the collision frequency. The migration of charged NPs is affected by the supporting electrolyte concentration and the faradaic current flow. A simplified model based on the NP transference number is introduced to explain the migrational flux of the NPs. Experimental collision frequencies and the transference number model also agreed with more rigorous simulation results based on the Poisson and Nernst−Planck equations.

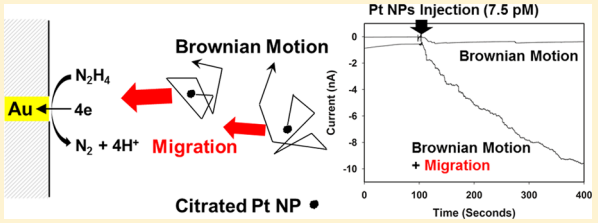


## 1. INTRODUCTION

We report a strong effect of migration in explaining single nanoparticle (NP) collision events of charged metal particles. Migration of the NP increases the particle flux to the electrode, resulting in an increase in the sensitivity of NP detection over previously reported current amplification (amperometric)[1−8] and potentiometric techniques.[9] In this previous work, NP mass transport only by diffusion (Brownian or random walk motion) was considered. This random process depends on the diffusion coefficient, which follows the Stokes−Einstein relation.[10]

Characterizing single particle collision events electrochemically has been suggested as a means of analysis of low concentrations, using particles as labels. However, the detection time can be quite long when the concentration of the particles in solution is low (e.g., attomolar or smaller) when the arrival of particles at the electrode only occurs by random motion (diffusion). To measure low analyte concentrations for analytical applications (e.g., in biomarker detection), a driving force of a single particle to the electrode is needed.[11] Extensive studies on analyte collection at electrodes have been carried out. Magnetic nanoparticles are frequently used to tag the analyte, because they can be attracted by a magnetic field.[12] Microfluidic systems utilize convection by pumping or elecroosmosis to produce flow through a microfluidic channel.[13] Migration of the nonconductive particles, e.g., latex or polystyrene beads, or silica particles, produce a decrease in the ferrocene methanol oxidation current of Pt ultramicroelectrodes (UMEs) by blocking the electroactive area.[14,15] However, the migration of conductive particles in collision experiments has not previously been considered.

Here, we show that catalytic metal NP collisions can be controlled by migration. Catalytic NPs colliding and adhering to an inert Au UME show steplike current increases upon collision events.[2] The total flux of particles is substantially enhanced by the migration effect, and the migrational flux of NPs was often larger than the diffusional flux in our experiments. Migrational collision frequencies were estimated based on the transference number of the NPs. A Multiphysics simulation was performed to calculate the NP flux using the Poisson and Nernst−Planck equations that take into account both diffusion and migration at the same time. Finally, a quick calculation method is suggested to estimate migrating NP frequency without simulation. The simulation results match well with both the experimental data and the suggested quick calculation results.

## 2. EXPERIMENTAL SECTION

**Reagents.** Sodium phosphate dibasic anhydrous ($Na_2HPO_4$, 99.5%), sodium phosphate monobasic monohydrate ($NaH_2PO_4·H_2O$, 99.5%), and potassium chloride (KCl, 99.6%) were obtained from Fisher Scientific (Pittsburgh, PA). Hexachloroplatinic acid hexahydrate ($H_2PtCl_6·6H_2O$, 99%) was obtained from Alfa Aesar (Ward Hill, USA). Hydrazine anhydrous ($N_2H_4$, 98%), citric acid (99.5%), L-ascorbic acid (99%), ferrocene methanol (97%), trisodium citrate dihydrate (99%), and sodium borohydride ($NaBH_4$, 98%) were obtained from Sigma-Aldrich. All chemicals were used as received. Millipore water (18 MΩ) was used in all experiments. Platinum

Received: December 21, 2012
Revised: February 27, 2013
Published: March 8, 2013

(99.99%) and gold (99.99%) wires, 10 $\mu$m in diameter, from Goodfellow (Devon, PA) were used to fabricate the UMEs.

**Preparation of UMEs.** Pt and Au UMEs were prepared following the general procedure developed previously. Briefly, a 10 $\mu$m diameter metal (Au, Pt) wire was sealed in a borosilicate capillary tube (0.75 mm i.d. 1.5 mm o.d., FHC, Brunswick, ME) after rinsing with ethanol and water. The electrode was then polished on an abrasive pad (Buehler, Lake Bluff, IL), followed by polishing to a mirror finish in alumina powder water suspension on microcloth pads (Buehler, Lake Bluff, IL). The surface area of electrodes was confirmed by standard redox electrochemistry of ferrocene methanol.

**Instrumentation.** The electrochemical experiments were performed using a CHI model 630 potentiostat and 920c potentiostat (CH Instruments, Austin, TX) with the three-electrode cell placed in a Faraday cage. A 3 mm diameter carbon rod was used as the counter electrode and the reference electrode was Ag/AgCl in a saturated KCl solution. All potentials are quoted versus Ag/AgCl. Pt NP mobility was measured by electrophoretic light scattering using a Zetasizer Nano ZS (Malvern Instruments, Malvern, UK).

**Preparation of Metal Nanoparticles (NPs).** The Pt NPs (diameter 32 ± 3 nm) solutions were prepared by the procedure reported previously.[9] A seed-mediated growth procedure was used to prepare stable citrate-capped large Pt NPs. Seed particles were prepared as follows. $H_2PtCl_6{\cdot}6H_2O$ (3.8 mM, 7 mL) was added to boiling water (90 mL) while stirring. After 1 min, 2.2 mL of solution containing 34 mM trisodium citrate and 2.6 mM citric acid was added, followed by a quick addition of freshly prepared sodium borohydride (21 mM, 1.1 mL). After 10 min, the solution was cooled to room temperature. For 32 nm particles, 1 mL of Pt seed solution was added to 29 mL of water with stirring. $H_2PtCl_6{\cdot}6H_2O$ (0.4 M, 0.045 mL) was added, followed by addition of 0.5 mL solution containing 34 mM trisodium citrate and 71 mM ascorbic acid. The temperature was slowly increased to the boiling point (~5 °C/min). The reaction time was 1 h with a reflux condenser. NPs were washed twice with water by precipitation in a centrifuge at 14 000 rpm for 10 min. A recent study showed that citrate adsorbed during synthesis (at 100 °C) is stable on the Pt NP even after the washing step.[16] From the measured zeta-potential value, ~−50 mV, we obtained approximately −190 charges per Pt NP (32 nm in diameter) in 5 mM monovalent supporting electrolyte solution.[17] For calculating the charge of NP, the interested reader is referred to Ohshima et al.[18]

**Multiphysics Simulation.** The simulation was performed by solving the Poisson and Nernst−Planck equations using COMSOL Multiphysics 3.5a software. The electrostatics and Nernst−Planck without charge neutrality modules were used. An adaptive free triangular mesh element was used. The mesh size at the UME surface was set to 5 nm. The following parameters were used at room temperature (298 K). In the Poisson equation the relative permittivity of the medium ($\varepsilon_r$) was set to 80, space charge density ($\rho$) was set as $\sum z_i C_i$ and $\varepsilon_0$ was the vacuum permittivity ($8.854 \times 10^{-12}$ F/m). Diffusion coefficients ($D$) of ions were assumed to be the ideal infinite dilution values; $D(Na^+) = 1.33 \times 10^{-5}$ cm$^2$/s, $D(HPO_4^{2-}) = 7.59 \times 10^{-6}$ cm$^2$/s, $D(H_2PO_4^-) = 9.59 \times 10^{-6}$ cm$^2$/s, $D(N_2H_4) = 1.39 \times 10^{-5}$ cm$^2$/s, $D(H^+) = 9.31 \times 10^{-5}$ cm$^2$/s, $D$(Pt NP) = $1.02 \times 10^{-7}$ cm$^2$/s.[19,20] The diffusion coefficient of the Pt NP was determined from the mobility that was measured by light scattering using a Zetasizer. Mobilities of ions ($u_i$) were calculated from the diffusion coefficients using the Einstein relation, $u_i = z_i D_i (F/RT)$,[10] where $z_i$ and $C_i$ represent the charge and concentration of the species $i$. $z_{NP}$ itself is not important in this simulation because it is already reflected in the $u_{NP}$.

## 3. EXPERIMENTAL RESULTS

We previously reported NP collision events using catalytic proton reduction with Pt NPs,[1] water oxidation with $IrO_x$ NPs,[3] hydrazine oxidation with Pt NPs,[2] and sodium borohydride oxidation on Au NPs.[4] Reported collision events were controlled by diffusion (Brownian motion) of the particles because of the relatively high supporting electrolyte concentration (e.g., 100 mM), which suppressed the migration effect. Under these conditions, the collision frequency of the NPs ($f_{diff}$) was determined from the flux of the adhering particles to the UME, $j_{diff}$, which is a function of $D_{NP}$, the diffusion coefficient of the particles, $C_{NP}$, the concentration of the particles and $r_0$, the radius of the UME disk electrode according to eq 1. Note that the frequency of NP is obtained simply by multiplying by Avogadro's number ($f_{diff} = j_{diff} N_A$).

$$j_{diff} = 4 D_{NP} C_{NP} r_0 \tag{1}$$

$$\text{valid NP ratio}(NP_{ratio}) = \frac{f_{diff,ex}}{f_{diff}} \tag{2}$$

The ratio in eq 2, $f_{diff,ex}/f_{diff}$, is an estimate of the number of observable collisions, and is obtained by comparing the collision frequency calculated with eq 1 and the experimental observed collision frequency, $f_{diff,ex}$, with 50 mM supporting electrolyte (where migration is negligible). This ratio (2) was ~13%. The observed diffusional collision frequency depends on the state of the surface of the NP and UME,[21] the NP contact with the UME, and NP size. For a more accurate calculation, a better estimate of the NP concentration is required. An analogous valid ratio of NP would also apply to the migrational flux of NP; this ratio must be considered when comparing the computed (or simulated) data to the experimental data.

One can increase the collision frequency by enhancing mass transport (e.g., by migration) of the NPs to the UME. To change the collision system from the diffusional dominance to one with a larger migrational component, (1) electrode potential, (2) faradaic current, (3) supporting electrolyte concentration (ionic strength), and (4) sign and magnitude of the particle charge should be considered.

The total flux of NPs is the sum of the migrational and diffusional fluxes, as shown in eq 3.

$$j_{total} = j_{diff} + j_{mig} \tag{3}$$

where $j_{total}$ is total flux of NP and $j_{mig}$ is migrational flux of NP. If we assume that $j_{diff}$ is given at steady state by eq 1, under the conditions of the experiments discussed here with low electrolyte, the total flux is mainly controlled by $j_{mig}$.

**Effect of Electrode Potential and Background Current.** Figure 1 shows Pt NP collision events using the hydrazine oxidation reaction at a Au UME at different electrode potentials and background currents that affected the Pt NP collision frequency. At −100 mV (background current ~1 nA) (Figure 1b) the frequency of the collision events was ~17 times larger than that at −150 mV (background current ~90 pA) (Figure 1a). The increase in the collision frequency can be attributed to the migration effect, because diffusional collisions are not affected by the electrode potential in the diffusion-limited


dx.doi.org/10.1021/jp3126494 | J. Phys. Chem. C 2013, 117, 6651−6657

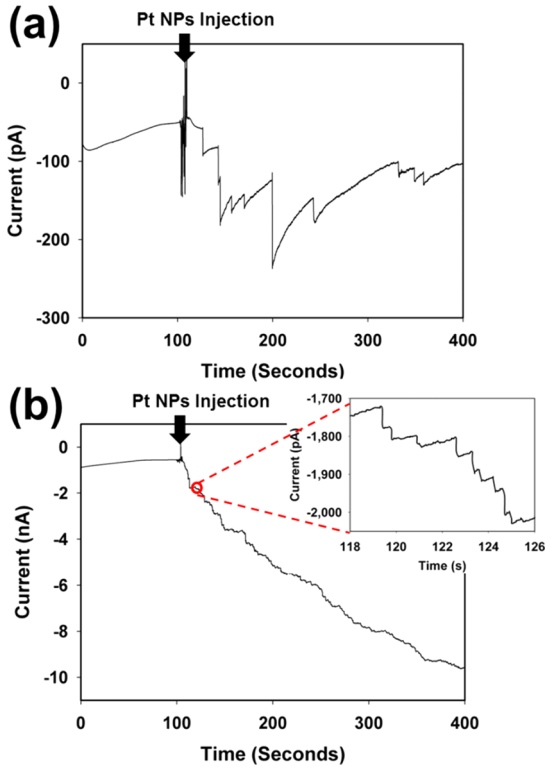


**Figure 1.** Chronoamperometric curves for single Pt NP (radius ~16 nm) collisions at the Au UME (radius 5 $\mu$m) in the presence of 7.5 pM Pt NPs in 5 mM phosphate buffer (pH 7.0) and 15 mM hydrazine. Applied potentials are (a) −0.15 V and (b) −0.1 V (vs Ag/AgCl). Data acquisition time was 50 ms.

region as indicated by eq 1. The two different collision frequencies with the same Pt NP concentration resulted from the increased anodic background current, ~10 times, so the flux of the negatively charged NPs increased (when the supporting electrolyte concentration was low (5 mM)) to supply the needed charge at the electrode to maintain electroneutrality (Scheme 1). With 50 mM supporting electrolyte, there was no migration effect at different electrode potentials. Deciding the proper supporting electrolyte concentration for a migration effect requires consideration of several factors, thus, one needs to do a simulation. For an estimate, the transference number of the NP can be used to determine the supporting electrolyte concentration needed to observe a migration effect, as discussed below.

**Insight from the Transference Number.** The transference number ($t_j$) indicates the fraction of the total current carried by the anions and cations in electrolysis as shown in eq 4.[22] The transference number of a NP represents the relative flux of charged NPs in the electrolyte solution.

$$t_j = \frac{|z_j| u_j C_j}{\sum_i |z_i| u_i C_i} \tag{4}$$

In considering the overall conduction, the NP transference number, $t_{NP}$, is usually neglected because its value is much smaller than those of the supporting electrolyte ions, $t_{Na^+}$ or $t_{H2PO4^{2-}}$, as shown in Scheme 1a. This indicates that the fraction of current in the bulk solution transported by Pt NPs is negligible. However, even this tiny transference number, $t_{NP}$, becomes important when the electrode reaction is controlled by the flux of NP to the electrode and the diffusional contribution to the mass transport of NPs is also tiny (because the NP diffusion coefficient value and the concentration are

**Scheme 1. (a) Migration Portion of Balance Sheet for the Electrochemical Cell, and (b) Pictorial Illustration of the Two Major Particle Fluxes of Diffusion (Brownian Motion) and Migration[a]**

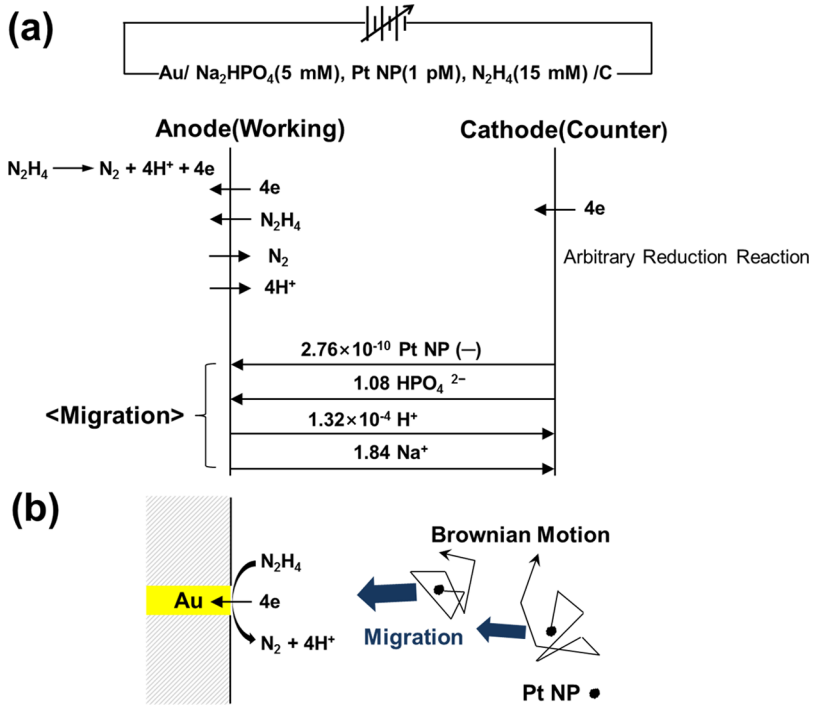


[a]Charge of Pt NP was assumed to be −190 for this estimation.


dx.doi.org/10.1021/jp3126494 | J. Phys. Chem. C 2013, 117, 6651−6657

very small). Under such conditions the NP migrational collision frequency becomes important.

**Origin of Migration: Effect of Current.** Migration (as also in electrophoresis) arises because of the effect of the electric field on a charged species in the bulk solution (Scheme 1a) and also near the electrode surface (i.e., within the diffusion layer) (Scheme 1b). This field develops because of the flow of faradaic current at the electrode, so that the migration effect depends on the magnitude of the faradaic current (which is a function of the electrode potential). Figure 2 shows three

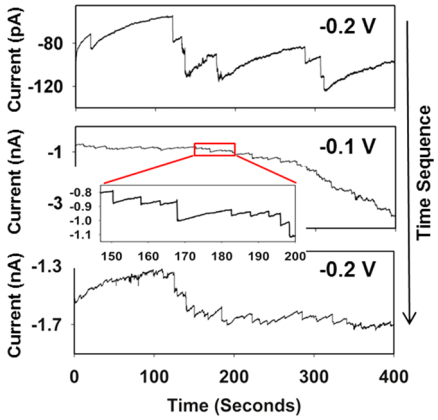


**Figure 2.** Chronoamperometric curves for single Pt NP (radius ~16 nm) collisions at the Au UME (radius 5 $\mu$m) at various potentials (−0.2, −0.1, and −0.2 V vs Ag/AgCl; by time sequence) in the presence of 7.5 pM Pt NPs, 5 mM phosphate buffer (pH 7.0), and 15 mM hydrazine. Data acquisition time was 50 ms.

consecutive Pt NP collision chronoamperograms with potentials −0.2 V, −0.1 V, and then back to −0.2 V applied in sequence. While the same potential was applied (−0.2 V), the observed collision frequency differed due to the history of the electrode. A clean Au UME in the first experiment only shows a few collision events within a 400 s window at −0.2 V with a small hydrazine oxidation current (~100 pA). At a subsequent more positive potential, −0.1 V, the oxidation current is larger. This mainly involves the kinetically controlled increase following Butler−Volmer behavior, and also the fact the electrode now has some Pt NPs attached from the earlier experiment. This increased oxidation current enhances the migrational flux of the negatively charged Pt NPs toward the Au UME and the collision frequency is larger. After many Pt NPs have stuck on the Au UME by collision events at −0.1 V, the attached catalytic Pt NPs increase the hydrazine oxidation current at −0.2 V on Au UMEs. When the potential is again switched to −0.2 V, the faradaic current at the Au UME is much larger (~1.5 nA) than in the initial −0.2 V experiment, and this leads to a larger collision frequency at −0.2 V.

**Effect of Supporting Electrolyte Concentration.** In addition to the current, the supporting electrolyte concentration is an important factor in migration, since it determines $t_{NP}$. One can expect the Pt NP collision frequency will decrease with an increase in the supporting electrolyte concentration. Figure 3 shows a Pt NP collision experiment at −0.1 and −0.05 V, applied potentials in the region where a large catalytic current difference exists between Au and Pt, with different supporting electrolyte concentrations. At a high concentration of the supporting electrolyte condition (50 mM) in Figure 3a, the Pt NP collision frequency was ~0.017 $pM^{-1}$ $s^{-1}$ for the first

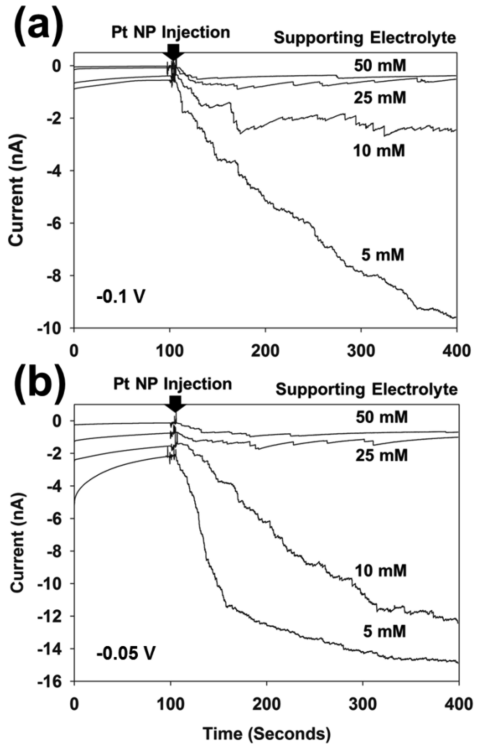


**Figure 3.** Chronoamperometric curves for single Pt NP (radius ~16 nm) collisions at the Au UME (radius 5 $\mu$m) with various phosphate buffer concentrations (50, 25, 10, and 5 mM; pH 7) in the presence of 7.5 pM Pt NPs and 15 mM hydrazine at −0.1 V (a) and −0.05 V (b) (vs Ag/AgCl). Data acquisition time was 50 ms.

100 s. By lowering the supporting electrolyte concentration to 5 mM, the Pt NP collision frequency increased to ~0.14 $pM^{-1}$ $s^{-1}$. This frequency difference is consistent with the about 10 times larger $t_{NP}$ at 5 mM compared with $t_{NP}$ at 50 mM supporting electrolyte concentration. Thus, the Pt NP collision frequency with 50 mM supporting electrolyte is controlled mainly by diffusion, with negligible migration of the Pt NPs, while at 5 mM the NP mass transfer is controlled mainly by migration. In Figure 3b, the faradaic current at the Au UME increased at the more positive potential, causing an increase in the NP collision frequency at all concentrations of supporting electrolyte. This demonstrates that adjustment of both the supporting electrolyte concentration and the applied potential is important in controlling the Pt NPs collision frequency at a Au UME.

**Collision Frequency Calculation.** The transference number indicates the fraction of current, $t_{NP}$, carried in the bulk solution by each species (where $t_{NP} = i_{NP}/i_{Total}$ and $i_{Total}$ is the total current flowing during a collision). The product $t_{NP}i_{Total}$ represents a measure of current by the NP. The current of NPs can be converted to the flux of NPs by multiplying by $1/(z_{PtNP}F)$. From the transference number and the faradaic current flow, one can estimate the flux of Pt NPs migrating to the Au UME per second by eq 5, where $i_{avg}$ is the average current flow at Au UME, $z_{NP}$ is the charge of Pt NP, and $F$ is the Faraday constant.

$$\text{migrational flux of Pt NP } (j_{mig}) = \frac{t_{NP}i_{avg}}{z_{NP}F} NP_{ratio} \quad (5)$$

The collision frequency was proportional to the average current, at a given supporting electrolyte concentration when


dx.doi.org/10.1021/jp3126494 | J. Phys. Chem. C 2013, 117, 6651−6657

the NP has the same transference number (i.e., at a given supporting electrolyte concentration), as shown in Figure 4.

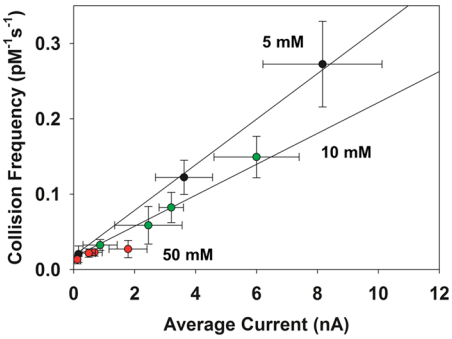


**Figure 4.** Collision frequency vs average current at three different phosphate buffer concentrations (5, 10, and 50 mM) at various potentials (−150, −100, −50, and 0 mV), which set the background current. Collision frequency was counted for the first 100 s after particle injection. The average current was obtained from integrating the charge and dividing by time. Data obtained by 3−5 replicate measurements.

The average current used in Figure 4 was obtained from the experimental result in Figure 3 by integrating the current to obtain the total charge and dividing it by the time. The slopes in Figure 4 represent the relative transference number magnitude. The relation between migrating NP and $i_{avg}$ implies eq 5 is qualitatively correct. The line for a smaller supporting electrolyte concentration has a steeper slope. With 50 mM phosphate buffer, diffusion dominates, and the collision frequency is almost independent of the current. The intercepts of these plots should represent the diffusional component. The applicability of eq 5 was studied by a model for calculating migration based on a Multiphysics simulation.

**Simulation.** A Multiphysics simulation was performed to obtain the expected collision frequency using a steady-state current (i.e., the average experimental current) at the UME. We assume the UME reaction is hydrazine oxidation ($N_2H_4 \rightarrow N_2 + 4H^+ + 4e$) and neglect mechanistic complications. The Poisson and Nernst−Planck equations, eqs 6 and 7, respectively, were used to describe the NP collision event under migration and diffusion.

$$-\nabla\varepsilon_0\varepsilon_r\nabla V = \rho \tag{6}$$

$$J_i(r, z) = -D_i\nabla C_i(r, z) - u_i C_i(r, z)\nabla V(r, z) \tag{7}$$

where $\varepsilon_0$ is the vacuum permittivity, $\varepsilon_r$ is the relative permittivity, $V$ is the electric potential, $\rho$ is space charge density, $J_i$ is the flux of each species, $D_i$ is the diffusion coefficient, $C_i$ is the concentration, and $u_i$ is the electrical mobility of the ionic species.

In the simulation the space dimension was taken as 2D axial symmetry, with electrostatics and nonconservative Nernst−Planck steady-state equation selected.[23] Simulation details are shown in the Experimental Section and the Supporting Information. Figure 5 shows the experimental collision frequency and simulated frequency as a function of the supporting electrolyte concentration. Every parameter value was the same for the two simulation sets except for the average current. The simulated Pt NPs collision frequencies agree fairly well with the two experimental data sets in Figure 3.

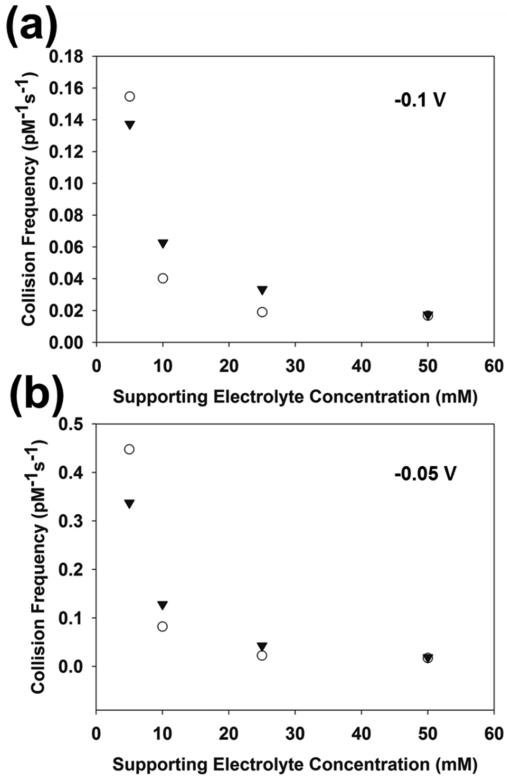


**Figure 5.** Experimental (triangles) and computed (circles. from Multiphysics simulation based on Poisson and Nernst−Planck equations) collision frequency as a function of the supporting electrolyte concentration at an applied potential of (a) −0.1 V and (b) −0.05 V. Average current in (a) is 3.4 nA (5 mM), 1.6 nA (10 mM), 0.66 nA (25 mM), and 0.4 nA (50 mM). Average current in (b) is 9.8 nA (5 mM), 3.6 nA (10 mM), 1.3 nA (25 mM), and 0.67 nA (50 mM). The average current and collision frequency were considered for the first 100 s after particle injection. Diffusion coefficient of ionic species used in here is obtained from the literature[19,20] which is described in detail in the Experimental Section.

**Comparison of the Simulation and the Simplified (Transference Number) Treatment for Calculating Collision Frequencies.** A simplified model for predicting conditions needed for a given collision frequency based on eq 5 is quicker and easier than carrying out the more rigorous Multiphysics simulation. One only needs the faradaic current for the electrode reaction ($A \rightarrow A^+ + e$; A is a uncharged oxidizable redox mediator (e.g., ferrocenemethanol, hydrazine)) that drives the migration and the transference numbers of all species in the starting solution. The collision frequency as a function of supporting electrolyte concentration computed from the simulation and from eq 5 with diffusion coefficients of A, $A^+$, and supporting electrolyte ions of $1 \times 10^{-5}$ cm$^2$ s$^{-1}$ and that of the Pt NPs of $1.02 \times 10^{-7}$ cm$^2$ s$^{-1}$ are plotted in Figure 6. The two results match quite well in this case. However, the transference number approach is not rigorously correct under all possible conditions, because it does not account for the role of electrogenerated species.[24] The transference number in the balance sheet assumes constant bulk solution concentrations and a steady state. However, it does not consider the production of ions by the faradaic reaction that leads to changes in the ionic concentrations (and hence the electric field) in the diffusion layer. Thus, in the example, the diffusion coefficient of $A^+$ governs the concentration profile near the electrode surface, as shown in Figure 7a. The NP collision


dx.doi.org/10.1021/jp3126494 | J. Phys. Chem. C 2013, 117, 6651−6657

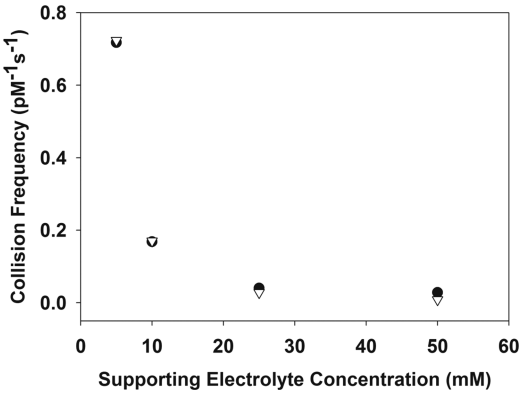


**Figure 6.** Quickly calculated and computer simulated (triangles from eq 5 ($NP_{ratio}$ = 1), and circles from Comsol simulations using Poisson and Nernst–Planck equations, respectively) collision frequency as a function of the supporting electrolyte concentration. Average current value used in both computations was 3.4 nA (5 mM), 1.6 nA (10 mM), 0.66 nA (25 mM), and 0.4 nA (50 mM), which is obtained from experimental results in Figure 3a. $D$(A), $D$($A^+$), and $D$(supporting electrolyte ions) are $1 \times 10^{-5}$ cm$^2$ s$^{-1}$ and $D$(Pt NPs) is $1.02 \times 10^{-7}$ cm$^2$ s$^{-1}$.

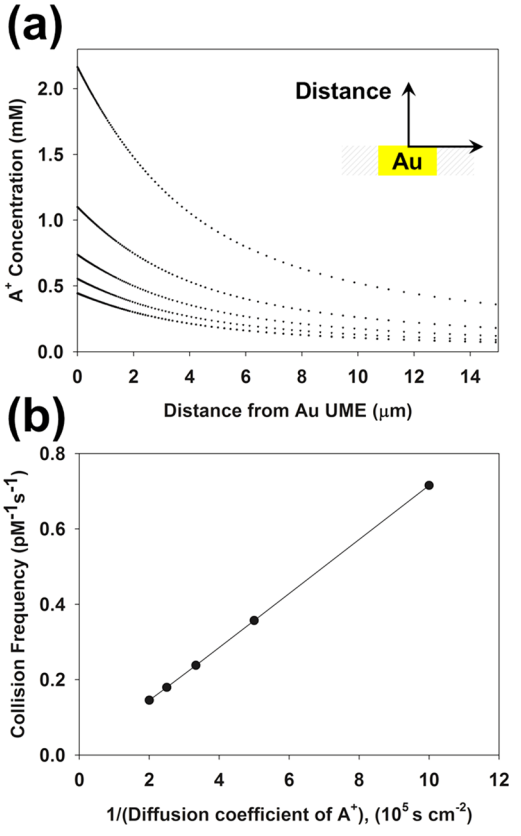


**Figure 7.** (a) Steady-state concentration profile of $A^+$ at the anode depending on diffusion coefficient of $A^+$ ($D$($A^+$), from top to bottom $1 \times 10^{-5}$, $2 \times 10^{-5}$, $3 \times 10^{-5}$, $4 \times 10^{-5}$, and $5 \times 10^{-5}$ cm$^2$ s$^{-1}$) and (b) NP collision frequency as a function of the diffusion coefficient of $A^+$. $D$(A) and $D$(supporting electrolyte ions) are $1 \times 10^{-5}$ cm$^2$ s$^{-1}$. $D$(Pt NPs) is $1.02 \times 10^{-7}$ cm$^2$ s$^{-1}$.

frequency is inversely proportional to the diffusion coefficient of $A^+$ as shown in Figure 7b, as obtained from Multiphysics simulation under the same conditions except for $D$($A^+$). Since the transference number balance sheet approach does not consider $D$($A^+$), it can lead to differences between the simulation and the transference number approaches. In the system under consideration, where the electrode reaction is hydrazine oxidation, one $H^+$ is produced per electron transferred. In a buffer solution, the generated $H^+$ reacts rapidly with the buffer base, and it is this ion that contributes to the electric field in the diffusion layer, so that the $D$ of the buffer ion should be considered rather than that of $H^+$. Figure 8

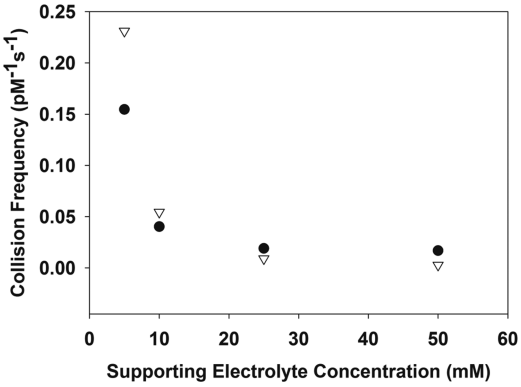


**Figure 8.** Computed (triangles from eq 5 ($NP_{ratio}$ = 1), circles from Comsol simulation based on Poisson and Nernst–Planck equations) collision frequency as a function of the supporting electrolyte concentration. Average current value used in both computations was 3.4 nA (5 mM), 1.6 nA (10 mM), 0.66 nA (25 mM), and 0.4 nA (50 mM) which is obtained from experimental results in Figure 3a. Diffusion coefficient of ionic species used here is obtained from the literature[19,20] which is described in detail in the Experimental Section.

shows the collision frequency obtained from the Multiphysics simulation and from eq 5 using the indicated $D$-values and mobility parameters. The results in Figure 8 show a deviation of about 30%.

**Guidelines for Designing a Migrational Collision System for Analytical Applications.** We have suggested the use of electrocatalytic NPs as labels in analytical applications, where observation of collisions could extend analyses to very small concentrations. Conditions where migration contributes significantly to the NP mass transfer and thus increasing the collision frequency increases the sensitivity of the analytical method. The conditions needed to maximize the collision current and frequency are the following: (1) transference number of NP should be maximized (i.e., high charge and small radius); (2) the charge of the redox reactant, A, for the faradaic reaction should be zero; (3) a large reactant concentration will enhance the faradaic current; (4) a small $D$ of the reaction product, $A^+$, or its product in a following reaction increases the electric field in the diffusion layer; (5) the sign of the NP charge must match the direction (anodic or cathodic) of the UME reaction; (6) low supporting electrolyte concentration.

On the basis of this study, citrated Pt NPs or Ag NP collisions, where the NPs are negatively charged, will not show a migration effect with the proton reduction as the NP reaction,[1,6] and an anodic electrocatalytic reaction is preferable. Similarly, negatively charged $IrO_x$ NP collisions with water oxidation will show a migrational effect. The Ag NP oxidative faradaic collision[6] is not subject to migration enhancement, because ideally no reaction happens until the Ag NP arrives at the electrode, so no current flows. It might be possible,


dx.doi.org/10.1021/jp3126494 | J. Phys. Chem. C 2013, 117, 6651–6657

however, to purposely introduce an electroactive reactant to create a background current in this case.

## 4. CONCLUSION

In electrochemical detection of single NP events on an electrode, the collision frequency can be increased under the right experimental conditions. The relative migration contribution for the Pt NP/Au UME/hydrazine oxidation system is affected by the supporting electrolyte concentration and the background current (determined by the applied potential). The NP collision frequency can be simulated by a Multiphysics program using the Poisson and Nernst−Planck equations and also calculated from a simple transference number-balance sheet approach from the mobility of the NP and the average total current. This technique could be used in designing the NP collision system for sensitive analytical detection (e.g., at the aM or lower level) with proper system design.

## ■ ASSOCIATED CONTENT

### Ⓢ Supporting Information

Simulation information. This material is available free of charge via the Internet at http://pubs.acs.org.

## ■ AUTHOR INFORMATION

### Corresponding Author

*Fax: 512-471-0088. Tel.: 512-471-3761. E-mail: ajbard@mail.utexas.edu.

### Present Address

⊥Department of Chemistry Education, Chonbuk National University, Jeonbuk 560-756, Republic of Korea.

### Notes

The authors declare no competing financial interest.

## ■ ACKNOWLEDGMENTS

We appreciate support from the Robert A. Welch Foundation (F-0021), the National Science Foundation (CHE-1111518), and the Department of Defense, Defense Threat Reduction Agency (Contract No. HDTRA1-11-1-0005), for support of the experimental studies. The content of the information does not necessarily reflect the position or the policy of the federal government, and no official endorsement should be inferred.

## ■ REFERENCES

(1) Xiao, X.; Bard, A. J. *J. Am. Chem. Soc.* **2007**, *129*, 9610−9612.
(2) Xiao, X.; Fan, F.-R. F.; Zhou, J.; Bard, A. J. *J. Am. Chem. Soc.* **2008**, *130*, 16669−16677.
(3) Kwon, S. J.; Fan, F.-R. F.; Bard, A. J. *J. Am. Chem. Soc.* **2010**, *132*, 13165−13167.
(4) Zhou, H.; Fan, F.-R. F.; Bard, A. J. *J. Phys. Chem. Lett.* **2010**, *1*, 2671−2674.
(5) Bard, A. J.; Zhou, H.; Kwon, S. J. *Isr. J. Chem.* **2010**, *50*, 267−276.
(6) Zhou, Y.-G.; Rees, N. V.; Compton, R. G. *Angew. Chem., Int. Ed.* **2011**, *50*, 4219−4211.
(7) Kahk, J. M.; Rees, N. V.; Pillay, J.; Tshikhudo, R.; Vilakazi, S.; Compton, R. G. *Nano Today* **2012**, *7*, 174−179.
(8) Kleijn, S. E. F.; Lai, S. C. S.; Miller, T. S.; Yanson, A. I.; Koper, M. T. M.; Unwin, P. R. *J. Am. Chem. Soc.* **2012**, *134*, 18558−18561.
(9) Zhou, H.; Park, J. H.; Fan, F.-R. F.; Bard, A. J. *J. Am. Chem. Soc.* **2012**, *134*, 13212−13215.
(10) Einstein, A. *Ann. Phys.* **1905**, *17*, 549−560.
(11) Gu, L.-Q.; Cheley, S.; Bayley, H. *Science* **2001**, *291*, 636−640.
(12) Haun, J. B.; Yoon, T.-J.; Lee, H.; Weissleder, R. *WIREs Nanomed. Nanobiotechnol.* **2010**, *2*, 291−304.
(13) Höltzel, A.; Tallarek, U. *J. Sep. Science* **2007**, *30*, 1398−1419.
(14) Quinn, B. M.; Hof, P. G.; Lemay, S. G. *J. Am. Chem. Soc.* **2004**, *27*, 8360−8361.
(15) Boika, A.; Thorgaard, S. N.; Bard, A. J. *J. Phys. Chem. B*. In press.
(16) Attard, G. A.; Ye, J.-Y.; Jenkins, P.; Vidal-Iglesias, F. J.; Herrero, E.; Sun, S.-G. *J. Electroanal. Chem.* **2013**, *688*, 249−256.
(17) Lyklema, J. *Fundamentals of Interface and Colloid Science*; Academic Press: London,1995; Vol. *II*, pp 3−21.
(18) Ohshima, H.; Healy, T. W.; White, L. R. *J. Colloid Interface Sci.* **1982**, *90*, 17−26.
(19) Lide, R. D.; Kehiaian, V. H. *CRC Handbook of Thermophysical and Thermochemical Data*; CRC Press: Boca Raton, FL, 1994.
(20) Karp, S.; Meites, L. *J. Am. Chem. Soc.* **1962**, *84*, 906−912.
(21) Xiao, X.; Pan, S.; Jang, J. S.; Fan, F.-R. F.; Bard, A. J. *J. Phys. Chem. C* **2009**, *113*, 14978−14982.
(22) Bard, A. J.; Faulkner, L. R. *Electrochemical Methods: Fundamentals and Applications*, 2nd ed.; John Wiley and Sons: New York, 2001; Chapter 2.
(23) Zhang, Y.; Zhang, B.; White, H. S. *J. Phys. Chem. B* **2006**, *110*, 1768−1774.
(24) Amatore, C.; Oleinick, A. I.; Svir, I. *ChemPhysChem* **2009**, *10*, 211−221.